MSP Dynamics Drives Nematode Sperm Locomotion

Charles W. Wolgemuth,* Long Miao,† Orion Vanderlinde,† Tom Roberts,† and George Oster‡
*University of Connecticut Health Center, Department of Cell Biology, Farmington, Connecticut 06030-3505; †Florida State University, Department of Biological Science, Tallahassee, Florida; and ‡University of California, Departments of Molecular & Cellular Biology, and Environmental Science, Policy, and Management, University of California Berkeley, Berkeley, California 94720-3112

ABSTRACT Most eukaryotic cells can crawl over surfaces. In general, this motility requires three sequential actions: polymerization at the leading edge, adhesion to the substrate, and retraction at the rear. Recent in vitro experiments with extracts from spermatozoa from the nematode *Ascaris suum* suggest that retraction forces are generated by depolymerization of the major sperm protein cytoskeleton. Combining polymer entropy with a simple kinetic model for disassembly we propose a model for disassembly-induced retraction that fits the in vitro experimental data. This model explains the mechanism by which disassembly of the cytoskeleton generates the force necessary to pull the cell body forward and suggests further experiments that can test the validity of the models.

INTRODUCTION

Fibroblasts crawl to close wounds, neutrophils track down pathogens, and metastatic cancer cells invade distant parts of the body. The crawling of these cells through the extracellular environment entails at least three separate physical processes: i), cytoskeletal extension at the front of the cell; ii), adhesion to the substrate at the cell front and release at the rear; and iii), pulling up the rear of the cell body (Abercrombie, 1980; Lauffenburger and Horwitz, 1996; Mitchison and Cramer, 1996). In most eukaryotic cells the organelle that orchestrates these processes is a cross-linked polymer network composed of actin filaments. Polymerization and addition of new actin filaments at the leading edge of the cell drives extension via a polymerization ratchet mechanism (Mogilner and Oster, 2003; Peskin et al., 1993) or gel swelling (Herant et al., 2003; Oster and Perelson, 1988, 1994). Transmembrane proteins, such as integrins, anchor cells to the substrate (Gaudet et al., 2003; Koo et al., 2002; Rahman et al., 2002). The mechanism by which force is generated to drive retraction of the cell body is still debated. Originally, this force was attributed to an actomyosin system similar to muscle (Huxley, 1973). However, Myosin II-null *Dictyostelium* cells are still capable of translocation (DeLozanne and Spudich, 1987; Knecht and Loomis, 1987). Mogilner and Oster suggested that the depolymerization of an actin meshwork could generate a contractile force to pull up the cell rear (Mogilner and Oster, 1996). Here we present a more detailed analysis of contractile force generation in a cell that lacks cytoskeletal protein motors. This problem has been addressed previously by finite element modeling (Bottino et al., 2001) and continuum modeling (Joanny et al., 2003; Mogilner and Verzei, 2003; Wolgemuth et al., 2004); the treatment here offers a microscopic explanation for the in vitro experiments on major sperm protein (MSP) force production (Miao et al., 2003) and its implications for nematode sperm locomotion.

Spermatozoa from nematodes, such as *Ascaris suum*, exhibit crawling motility strikingly similar to those of other crawling cells (Fig. 1). Although they show all three characteristics of crawling, they do not possess an actin cytoskeleton. Rather, the nematode sperm utilizes a gel of an unrelated polymer, MSP. As in actin-based cells, polymerization of MSP at the leading edge of the lamellipod produces the force necessary to push out the front of the cell (Italiano et al., 1996). Unlike actin, MSP forms nonpolar filaments (Bullock et al., 1996), and molecular motors have not been identified. These results strongly suggest that the dynamics of the MSP network is responsible for both protrusive and retraction forces in crawling sperm cells. Recent in vitro experiments using cellular extracts from *A. suum* spermatozoa implicate disassembly of the MSP network as the force-generating mechanism driving translocation of the cell body (Miao et al., 2003). In these experiments, vesicles made from the membrane of *A. suum* sperm in the presence of sperm cytosol induce polymerization of a ''comet tail'' cylinder of MSP that pushes the vesicle (Italiano et al., 1996), similar to the motion of ActA coated beads in the presence of actin (Cameron et al., 1999). Retraction forces could be induced in the MSP gel by addition of *Yersinia enterocolytica* tyrosine phosphatase (YOP) to the cell-free extract of sperm (S100), although the comet tails in buffer solution showed only slight retraction (Miao et al., 2003). Frames from movies of this process in the presence of S100 + YOP or KPM buffer are shown in Fig. 2, *A* and *B*.

In nematode sperm, MSP forms a polyelectrolyte gel composed of a network of interconnected positively charged filaments surrounded by cytosolic fluid. This gel coexists in two forms: a distributed gel consisting of MSP filaments, and condensed regions of filaments (also called ''fiber

Submitted October 8, 2004, and accepted for publication January 19, 2005.

Address reprint requests to George Oster, E-mail: goster@nature.berkeley.edu.

0006-3495/05/04/2462/10 $2.00

doi: 10.1529/biophysj.104.054270

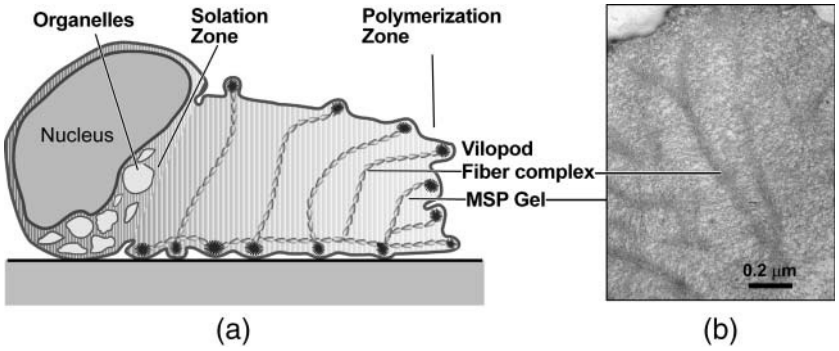

FIGURE 1 The *Ascaris suum* sperm. (*a*) Profile view diagram of a sperm crawling to the right. (*b*) Micrograph showing the dispersed and fiber complex phases of the MSP gel.

complexes,'' ''bundles,'' or ''ribs'') that span the lamellipod from the leading edge to the cell body (see Fig. 1). The organization of the filaments throughout the lamellipod appears to be mostly isotropic; however, images taken by electron microscopy show a bottle brush structure in the fiber complexes (Sepsenwol et al., 1989), suggesting that the filaments may be more ordered in these regions. The in vitro experiments on vesicles suggest that solation of this MSP gel induces contractile forces that pull the cell body forward. In Fig. 2 *C* we have replotted the original data from (Miao et al., 2003). The closely overlapping curves show that there is a direct correlation between the retraction (change in length, ΔL) and the disassembly (change in optical density, ΔOD) that is independent of the solution chemistry. In the Appendices we include a brief recapitulation of the methods used for these measurements.

In this article we present a model that explains the experimental data of vesicle retraction, and by extension, how disassembly of the MSP gel network can produce the contractile force necessary to pull the cell body forward during crawling. As neither the persistence length of the MSP filaments nor their organization in the in vitro comet tails is known, we begin by modeling the mechanical behavior of the MSP network using two separate physical descriptions: i), a polyelectrolyte gel stress based on microscopic parameters and the MSP polymer volume fraction, and ii), a bundled network of semiflexible MSP filaments. Coupling these mechanical models to a simple kinetic model for disassembly produces a mechanochemical engine that can fit the in vitro experiments on sperm extracts. Finally, we suggest further experiments to test the models.

Forces generated by MSP depolymerization and bundling

In this section we describe how MSP polymerization and depolymerization can generate directed forces that drive cell protrusion at the cell's leading edge and retraction at the trailing edge. The cytoskeleton of nematode sperm is composed of a large number of interconnected MSP filaments that constitute a polyelectrolyte gel. The volume of such gels is determined by the equilibrium between four forces (see Fig. A1 and Eq. 2): i), the entropic tendency for the gel filaments to diffuse outwards; ii), the ''counterion pressure'' that tends to inflate the gel (The tendency of the counterions to diffuse out of the gel sets up a countervailing electric field at the gel surface (the Donnan potential). This ''electrostatic membrane'' prevents the ions from leaving the gel, so the counterions can be treated as a gas tending to inflate the gel (see the Appendices)); iii), the entropic elasticity of the gel filaments that tends to resist expansion, and iv), the attractive interactions between the filaments that also tend to hold the

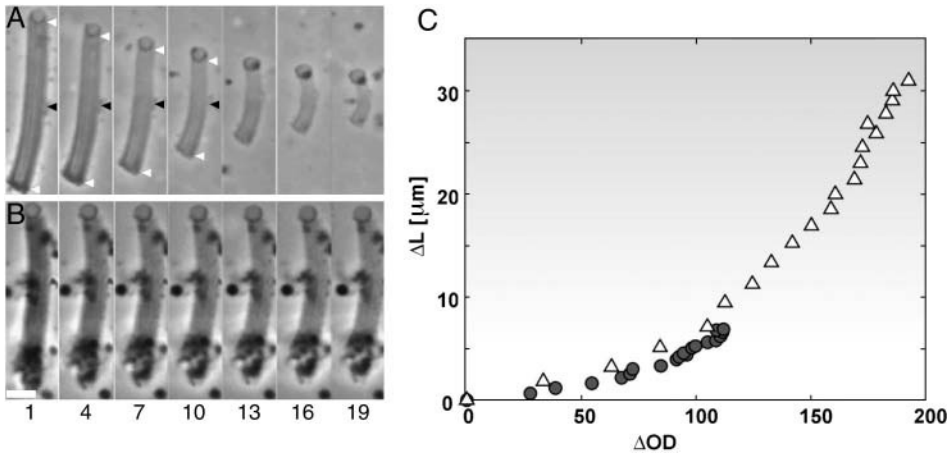

FIGURE 2 Experimental images of the vesicle propulsion experiments of (Miao et al., 2003). (*A*) A photographic sequence showing the depolymerization and contraction of an MSP cylinder in cell extract with *Yersinia enterocolytica* tyrosine phosphatase (YOP). (*B*) A similar fiber in KPM buffer (0.5 mM $MgCl_2$, 10 mM potassium phosphate, pH 6.8). The numbers indicate a succession of time points in minutes. (*A* and *B*) Bar = 5 μm. (*C*) The change in optical density (ΔOD) with length of an MSP fiber in KPM buffer shows that depolymerization is accompanied by contraction. Triangles are for media containing cell-free sperm extracts and YOP; circles are for media of KPM buffer. Data from Miao et al. (2003).

gel together. The MSP gel is not homogeneous for electron micrographs of MSP from *A. suum* show two different conformations for MSP aggregation in vivo: i), as an isotropic meshwork, and ii), as fiber bundles (see Fig. 1 *b*) (Roberts and Stewert, 1997). We will refer to these two states of the MSP cytogel as the meshwork phase and the bundle phase. In the meshwork phase filament alignment appears random and isotropic. Lateral association of MSP filaments leads to bundle formation. In this case, MSP alignment is more ordered and regions of the gel are dense and appear darker in light microscope images (Fig. 1 *b*). In both configurations cross-linking of the filaments increases the rigidity of the overall structure and locks out entropic degrees of freedom. Solation involves breaking chains in the meshwork phase, or unbundling filaments in the bundle phase. When the structure solates, the rigidity of the structure decreases and the gain in filament entropic freedom drives retraction of the network. The energy sources for contractile and protrusive work are the free energies of polymerization in the meshwork phase and the lateral association free energy of the filaments in the bundle phase. This is illustrated in Fig. 3.

Retraction forces induced by solation

In the Appendices we develop a mathematical model to describe the disassembly of the MSP gel and the mechanism of force production. Here we give a qualitative description of the model. Solation of the gel phase proceeds in two steps. First, chains are severed from the bulk gel creating chains with free ends as shown in Fig. 3 *b*. Second, the free ends depolymerize into monomers, which are subsequently recycled, a process we do not treat here.

Let M_c denote the mass of polymer gel, and M_f the mass of stress-free polymer chains created by severing. The total mass of polymer in the system is $M_t = M_c + M_f$. Solation takes place in two steps:

$$M_c \underset{\text{severing}}{\overset{k_c}{\rightarrow}} M_f \underset{\text{depolymerization}}{\overset{k_f}{\rightarrow}} m,$$

Here m is the mass of monomer, k_c is the rate for filament severing, and k_f is the rate constant for depolymerizing free polymer into monomers. A complete description of the kinetics is in the Appendices.

The total mass of the polymer in an isotropic gel is $M = \rho_m \phi V$, where ρ_m is the density of a monomer and ϕ is the volume fraction (i.e., the ratio of the volume of polymer to the total volume, V, of the gel). The surrounding fluid and counterions generate a pressure that swells the polymer, while the elasticity of the gel filaments as well as polymer-polymer interactions work to contract the gel. The coordinated effect of these four forces define the stress in the gel (For a mathematical description of the stress see Eq. 2 in the Appendices and English et al., 1996a; Wolgemuth et al., 2004).

In the absence of external forces, the total stress is zero at equilibrium. Indeed, this condition defines the equilibrium volume fraction of the gel. The network elasticity is set by the number of chains with both ends connected into the meshwork (Fig. 3) and by the average length of those chains.

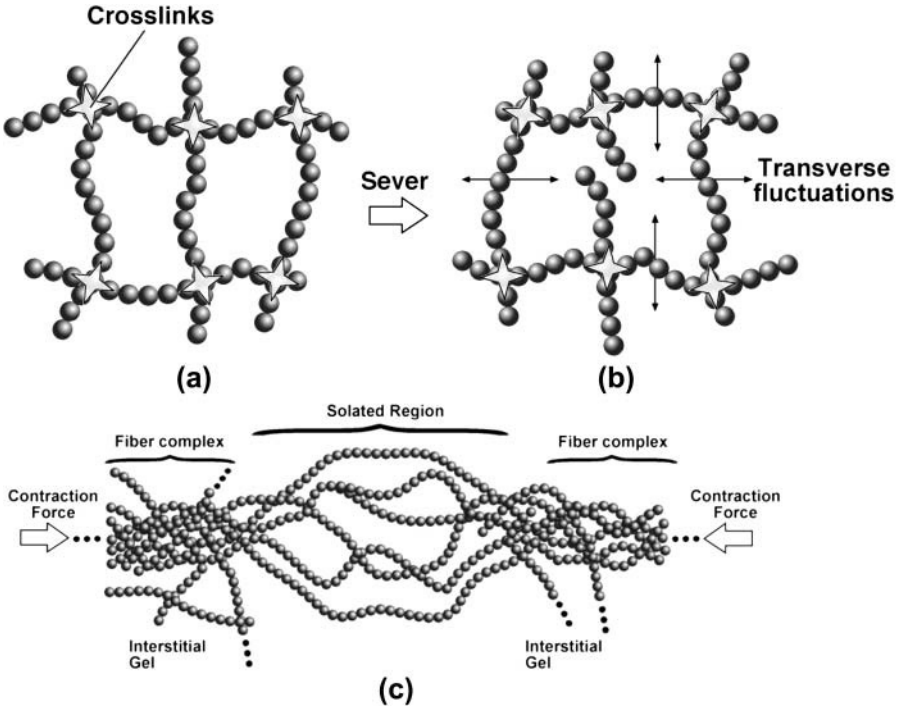

FIGURE 3 (*a*) In the distributed phase of the MSP gel, breaking a polymer chain by removal of a monomer increases the entropic freedom of branches so that their transverse fluctuations draw the cross-links closer together. Spheres correspond to monomers and crosses denote cross-links. In panel *b* the central connected chain has been severed, creating two free ends and leaving all cross-links intact. (*c*) A fiber bundle that begins to dissociate in the lamellipod creates MSP filaments whose persistence length is much shorter than the bundle. The transverse fluctuations of these filaments generate a contractile stress in the filament bundle.

As the gel solates, the number of connected chains decreases, the average length of chains increases, and the gel becomes more compliant. As the length of the connected chains increases the gel becomes more sensitive to thermal fluctuations: longer chains can fluctuate more and this draws their ends closer together. Thus, as a gel solates the remaining connected filaments tend to contract the gel. Because the gel is connected to the substratum via contact loci, the stress generated by the solation can exert traction to move the cell.

Filament bundles behave similarly. The elasticity of a single polymer filament is described by its total contour length, L_T, and its persistence length, $\ell_p = k_B T \cdot B$, where B is the bending modulus. The ratio L_T/ℓ_p defines the stiffness of the polymer. When $L_T/\ell_p \gg 1$, the filament is floppy, and when $L_T/\ell_p \leq 1$, the filament is fairly rigid.

Lateral adhesion of filaments produces a fiber bundle with a cross-sectional area proportional to the number of filaments. From elasticity theory the effective persistence length of the composite filament bundle is roughly proportional to the square of the cross-sectional area: $\ell_p \propto A^2$. Therefore, the rigidity of the filament bundle is proportional to the square of the number of attached filaments, $L_T/\ell_p \propto N^2$. We model the disassembly of the filament bundle as a two-step process. First, filaments detach from the bundle; as the bundle loses rigidity it contracts due to gain in entropic freedom. Second, the separate filaments depolymerize into monomers. Using an entropic model for semiflexible filaments, it is possible to calculate the disassembly-induced contraction of the polymer bundle (see the Appendices; MacKintosh et al., 1995).

RESULTS

As the persistence length of MSP and the configuration of the MSP filaments in the in vitro experiments are unknown, we explored both the meshwork and bundle models as possible mechanisms for retraction. To compare the model derived above with the experiments in Miao et al. (2003), we first convert length and OD versus time to MSP mass and volume fraction versus time using the relation between mass and volume described above and Beer's law to relate the optical density to the volume fraction (see the Appendices). The results are shown in Fig. 4, *top panels*. Both the mass and the volume fraction decrease as a function of time; however, the mass decreases faster than the volume fraction, which requires an overall contraction of the MSP network. Using the mass-versus-time plot, we fit the parameters k_f and k_c in KPM buffer and in S100 supplemented with YOP. We find good fits with a value of $k_f = 0.5\ \text{min}^{-1}$ and $k_c = 0.05\ \text{min}^{-1}$ in KPM buffer and $k_c = 0.14\ \text{min}^{-1}$ in S100 + YOP (Fig. 5). The depolymerization rates for MSP comet tails have not been measured; however, the value found for k_f is roughly comparable to the depolymerization rate for actin measured in crude extracts and in vivo (Theriot et al., 1994; Watanabe and Mitchison, 2002).

Next we modeled the change in volume fraction, ϕ, with time using the determined values for k_c and the two physical models for the solation of the MSP network (see Fig. 3 and the Appendices). We find good agreement between the model and the data (Fig. 4, *top right*). As shown in the figure, the volume fraction of the MSP gel decreases during the first

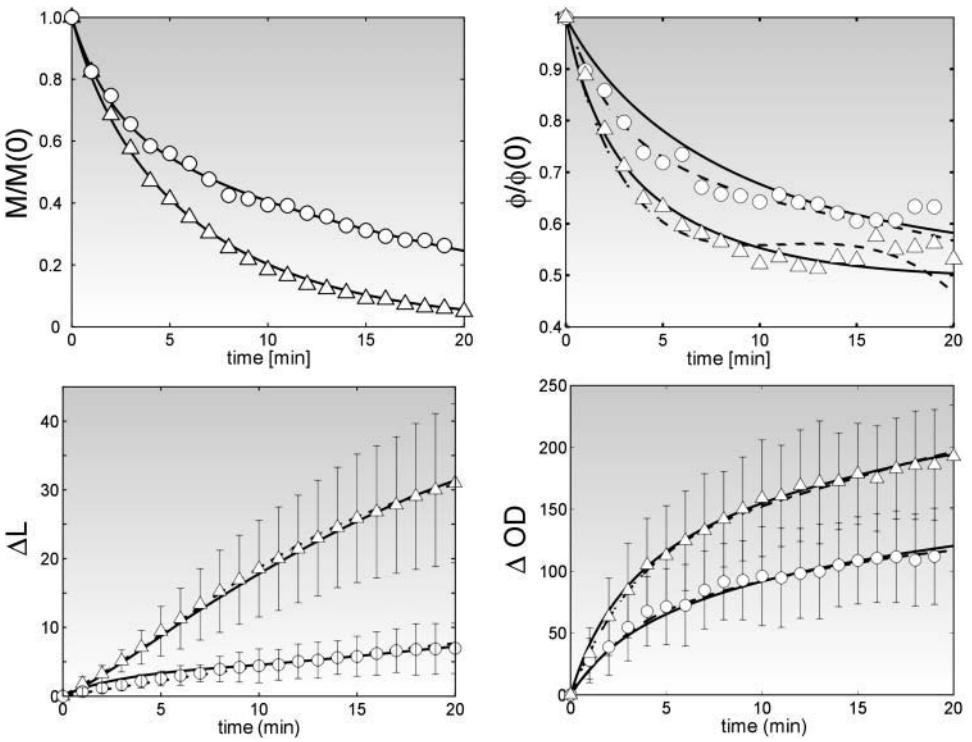

FIGURE 4 Model fits to data taken from Miao et al. (2003). (*Top left*) MSP polymer mass versus time. Solid line is a fit to the mass kinetic model, and circles (KPM buffer media) and triangles (s100 and YOP media) represent a replotting of the data from Miao et al. (2003) using equations derived in the Appendices. (*Top right*) MSP volume fraction versus time. Solid line is a fit to the gel retraction model, dashed line is a fit to the bundling model, and circles (KPM buffer media) and triangles (s100 and YOP media) represent a replotting of the data from Miao et al. (2003) using Eq. 8. (*Bottom left*) Cumulative loss in length of an MSP fiber versus time. (*Bottom right*) Cumulative loss in optical density versus time. (*Bottom panels*) Triangles show data for fibers in media with YOP and cytosol. Circles are for fibers in KPM buffer. Solid lines are fits using the gel retraction model and dashed lines are fits using the bundling model.

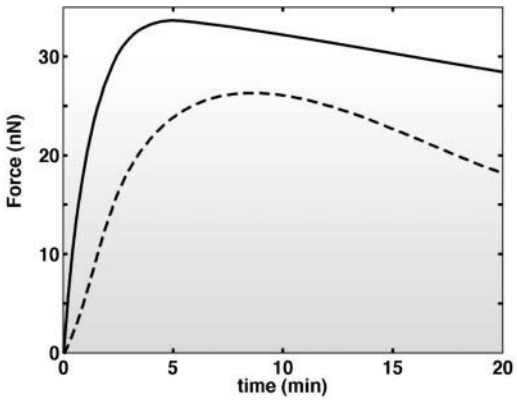

FIGURE 5 Plot of force versus time derived from the model (Eq. 3 in the Appendices) when both ends of the MSP fiber are held fixed. The solid line shows the result for the MSP fiber in KPM buffer. The dashed line is the result for the MSP fiber in cell-free extract and YOP.

10 min and then tends to flatten out for both solution chemistries. In S100 supplemented with YOP, this decrease is more rapid than in KPM buffer. The parameter values used in the model are listed in Table 1. To compare the values calculated in this manner with the original data, we plot the change in length and optical density using the model. Fig. 4, *bottom panels*, show that both solation models capture the disassembly and retraction of the MSP gel.

The experiments that have been done so far show that disassembly can produce retraction in MSP fibers associated with vesicles. However, these experiments do not show directly that this retraction can produce sufficient force to pull the cell body forward during crawling. The model suggests an experiment that can test the force production by disassembly of the MSP network. (Miao et al., 2003) observed that a bead could be attached to the MSP fiber and pulled along with the retracting fiber. If a bead is adhered to each end of the MSP fiber, the force required to prevent retraction can be measured using micromanipulation techniques such as flexible handles (Marcy et al., 2004). If we assume that under these conditions, the volume of the MSP fiber stays fixed, then $\phi = M/\rho_m V$. The force required to hold the ends is just the magnitude of the elastic stress times the cross-sectional area of the MSP tail (for further details, see the Appendices).

TABLE 1 Parameters and numerical values used in the model

Symbol	Definition	Value and units
V_m	Volume of a monomer	1 nm^3 (English et al., 1996a)
ϕ_0	Material parameter settingunstressed volume fraction	~0.1 (English et al., 1996a)
k_BT	Thermal energy	≈4.1 pN nm
N_A	Avogadro's number	6.02×10^{23}
$N_x(0)$	Initial number of monomers between cross-links	60 (fit from model)
χ	Flory interaction parameter	0.7 (English et al., 1996a)
α	Effective number of charges permonomer	~0.13 (assumed)
C_b	Bath ion concentration	~0.073 M (assumed)
k_f	Free chain depolymerization rate constant	0.5 min^{-1} (fit from model)
k_c	Connected chain depolymerization rate constant	0.05 min^{-1} in KPM buffer (fit from model) 0.14 min^{-1} in YOP and s100 (fit from model)
$M_c(0)$	Initial mass in connected chains	0.6 M(0) (fit from model)
$M_f(0)$	Initial mass in free chains	0.4 M(0) (fit from model)
$M(0)$	Total initial MSP mass	Actual value not needed
ε	Extinction coefficient	Actual value not needed
β	N_x rate constant	80/M$_c$(0) (fit from model)
A	Cross-sectional area of MSP comet tail	10 μm^2 (from experiment)

Fig. 5 shows that the maximum force on the comet tail produced by fiber depolymerization does not depend strongly on the presence of YOP. Both situations produce a maximum force ~30 nN. This force is comparable to the experimentally measured force required to halt crawling in keratocytes (Oliver et al., 1994). However, because a crawling cell traverses a cell length per minute, the physiological translocation force per bundle is more reasonably estimated by the force generated during the first minute. This force is found to be 5 nN in KPM buffer and 15 nN for S100 + YOP. Interestingly, the model predicts a slower rise for the force produced in the presence of YOP where the network is being disassembled faster. This result is somewhat counterintuitive because it seems that faster disassembly should lead to faster force production. However, the elastic strength of the network depends strongly on the cross-link density, whereas the stress depends strongly on the volume fraction, ϕ. In KPM buffer, the MSP mass that is contained in the free chains quickly depolymerizes, but cross-links and connected chains stay intact. Therefore, the elasticity of the network remains strong, while entropic pressure from the free chains is removed driving network contraction. When YOP is added, cross-links are broken more quickly. Therefore, the elasticity of the network decreases and free chain polymer is removed from the system at comparable rates; therefore, force production is slower. At longer times, the force decreases as the elasticity in the network is degraded.

This force dynamics may play a role in nematode sperm translocation. As the cell crawls, new polymer is added at the leading surface and old polymer gets progressively closer to the rear of the cell where disassembly induces the retraction necessary to pull the cell body forward. At the front of the cell, adhesion to the substrate is strong. Therefore, applying large forces at the leading edge are ineffective—or even counterproductive—if the force is large enough to break the adhesion to the substratum. Slower force production in the presence of YOP shifts the location of strong retraction toward the rear of the cell where it is most effective in pulling the cell body forward.

DISCUSSION

We have presented a model to describe the mechanism by which retraction forces are produced in crawling nematode sperm. We show that removing mass from a gel or fiber bundle produce contractile stresses that generate sufficient force to pull the cell body forward. The time dependence of the comet tail mass in vesicle experiments is fit well with a model that assumes that YOP controls the rate at which connected chains are converted to free end chains. This result suggests that YOP regulates filament severing or degradation of cross-links. The model provides quantitative agreement with in vitro experiments on cellular extracts where disassembly of the MSP network generates contractile forces. We suggest new experiments that can test the validity of the model.

As myosin is not required for translocation in *Dictyostelium* (DeLozanne and Spudich, 1987; Knecht and Loomis, 1987), a similar solation/retraction process in actin-based cells may generate the force required to haul the cell body forward during crawling. The natural depolymerization of actin from the cytoskeletal network and from comet tails behind moving *Listeria monocytogenes* and ActA coated beads is consistent with this idea (Cameron et al., 2000). At physiological conditions the elastic energy of actin networks is predominantly entropic (Gardel et al., 2004). Therefore, even though MSP may be more flexible than actin, it is reasonable to assume that solation will act qualitatively similar in these two polymer networks. Quantitative measurements of the rate of contraction to the rate of disassembly in any of these systems, similar to that done in vitro with MSP, would provide a method to test this hypothesis.

Just as depolymerization and unbundling can lead to retraction forces, in a similar fashion, protrusive forces could also be generated by using the free energy of bundling MSP filaments to weave fibers with larger bending moduli, or persistence lengths. Replacing the disassembly model we have presented here with a kinetic description of polymerization suggests a novel mechanism by which protrusive force can be generated at the leading edge of the crawling cell. A brief description of this bundling protrusion model is given in the Appendices with a more detailed description to be presented elsewhere. Recent experiments have shown that fascin-mediated actin bundling is required for protrusion of filipodia in melanoma cells, and similar actin bundling contributes significantly to force generation in *Listeria* motility (Brieher et al., 2004; Svitkina et al., 2003). Thus bundling may play a role in actin-based protrusion as well.

APPENDIX A: MEASUREMENTS OF THE MSP FIBERS

Images of the MSP fibers were obtained with a Ziess Axiovert 35 microscope (Carl Zeiss, Thornwood, NY) equipped with an oil immersion 63× Plan Neofluar objective and an Orca 12-bit digital camera (Hamamatsu, Bridgewater, NJ) using phase contrast optics, were captured at 5-s intervals. Measurements of fiber length, diameter, and optical density were obtained with Metamorph software. For optical density measurements, values were obtained by measuring optical density in grayscale units from a uniform region of the fiber (with care taken to exclude longitudinal stripes or irregularities due to debris clinging to the fiber). Images of the frames lacking fibers or other objects were used to obtain values for background subtraction. Optical densities were reported as grayscale values. Data plotted represent the mean over tens of fibers.

APPENDIX B: DEPOLYMERIZATION FORCES IN MSP GELS

A gel is a number of polymer chains connected by cross-links. Let ϕ denote the volume fraction of the MSP gel, so that in a unit volume of the gel a fraction of the space, ϕ, is occupied by the polymer and the remaining space is the fluid, $(1 - \phi)$. If the volume fraction is constant throughout the gel, the total mass of polymer in the gel fraction is

$$M = \rho_m \phi V, \tag{1}$$

where ρ_m is the density of a monomer and V is the volume of the gel. Depolymerization of the gel will decrease M and ϕ. Here we show that the volume of the gel, V, decreases if the stresses generated by depolymerization exceed the gel osmotic pressure.

The stress in a volume of gel, σ, is the sum of four effects (see Fig. A1). The elasticity of the polymers acts to restore the network to its mechanical equilibrium volume fraction, ϕ_0, whereas attractive polymer interactions tend to collapse the gel. Entropic mixing with the fluid and osmotic pressure generated by the polymer counterions induce swelling. The competition between these effects drives ϕ to an equilibrium value. External forces deform the gel creating stress in the network that changes the volume fraction. Electron microscopy images show MSP filaments that are often bent at lengths of tens of nanometers, suggesting that this length is comparable to the persistence length of MSP (Bottino et al., 2001). Therefore, it is reasonable to treat the MSP filaments composing the cytoskeletal meshwork as flexible. Using a Flory-Huggins free energy (Flory, 1953), and assuming an isotropic and homogeneous gel, the stress is a function solely of the volume fraction:

$$\left(\frac{V_m}{k_B T}\right)\sigma_{ij} = \left(\underbrace{-\ln(1-\phi) - \phi}_{\text{mixing}} - \underbrace{\chi\phi^2}_{\substack{\text{polymer}\\ \text{interaction}}} + \underbrace{\frac{1}{N_e}\left(\frac{1}{2}\phi - \phi_0^{2/3}\phi^{1/3}\right)}_{\text{elasticity}} - \underbrace{2N_A V_m (C_{ion} - C_b)}_{\substack{\text{counterion}\\ \text{pressure}}} \right)\delta_{ij}. \tag{2}$$

Here N_A is Avogadro's number, V_m is the volume of a monomer, k_B is Boltzmann's constant, and T is the temperature, and δ_{ij} is the identity matrix.

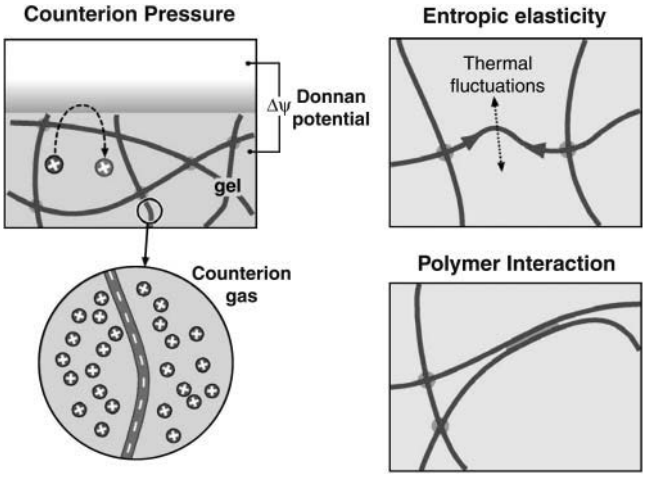

FIGURE A1 Forces in a polyelectrolyte gel (see Eq. 2).

χ is the Flory parameter that measures the interaction energy between polymer chains (Flory, 1953). The total force generated at the ends of a constant volume fraction gel comet tail is found from this stress using

$$\mathbf{F} = A(\hat{\mathbf{n}} \cdot \sigma \cdot \hat{\mathbf{n}}), \tag{3}$$

where A is the cross-sectional area of the comet tail and $\hat{\mathbf{n}}$ is the unit vector parallel with the axis of the tail.

The elasticity of the network depends on the effective number of monomers between cross-links, N_e, and a reference volume fraction, ϕ_0 (for a detailed derivation of the stress see English et al., 1996b; Flory, 1953; Wolgemuth et al., 2004, and the Appendix). The counterion pressure depends on the density of ions in the gel, C_{ion}, and the bath ion concentration, C_b.

Solation of the network will change N_e and ϕ_0 (Wolgemuth et al., 2004), and so we require a model for network severing. The polymer network contains two kinds of chains: those where both ends terminate in a cross-link, and those where one end is free (see Fig. 3). Let M_f be the mass of polymer in the free chains and M_c the mass in connected chains. The simplest model assumes that connected chains get broken and are transformed into free chains, which then depolymerize. The kinetics for this model are

$$\begin{aligned} \frac{dM_c}{dt} &= -k_c M_c \\ \frac{dM_f}{dt} &= k_c M_c - k_f M_f, \end{aligned} \tag{4}$$

with rate constants k_c and k_f. These equations can be solved analytically:

$$\begin{aligned} M_c &= M_c(0)e^{-k_c t} \\ M_f &= \left(M_f(0) + \frac{k_c}{k_c - k_f} M_c(0)\right) e^{-k_f t} - \frac{k_c}{k_c - k_f} M_c(0) e^{-k_c t}, \end{aligned} \tag{5}$$

where the total mass is $M = M_c + M_f$.

When no external forces act on the gel, $\sigma = 0$ at equilibrium. For a gel the size of the MSP fibers ($\sim$5 μm in diameter), the relaxation time is of order of seconds. From experiments, the timescale for depolymerization of the MSP network is of order minutes. Therefore, we will assume that depolymerization of the gel occurs on a timescale much slower than the relaxation of the gel. We also assume that the only parameters affected by depolymerization of the network are N_e. Thus if we know the kinetics for N_e, then solving the zero stress condition gives us the dynamics of ϕ. The contraction of the gel can then be computed from the change in volume, where $V = M/\phi$. Because N_e is the effective number of monomers between cross-links, as cross-links are destroyed, N_e increases. The rate that cross-links are destroyed should be proportional to the rate that the connected chains are broken. Therefore, we assume the simple kinetics

$$\frac{dN_e}{dt} = \beta k_c M_c, \tag{6}$$

where β is a constant. Using Eq. 5,

$$N_e = N_e(0) + \beta M_c(0)(1 - e^{-k_c t}). \tag{7}$$

To connect the theory with the experiments, M and ϕ need to be converted to length, L, and optical density, OD. We use the Beer-Lambert law,

$$OD = \varepsilon \phi r, \tag{8}$$

where ε is the extinction coefficient and r is the radius of the cylindrical MSP fiber and also the average thickness of MSP gel that the light travels through. Using Eq. 1 and the assumption that the comet tail is a cylinder, the mass of MSP is

$$M = \rho_m \phi(\pi r^2 L). \tag{9}$$

Experimentally, it is observed that radial strain ($\Delta r/r$) is proportional to longitudinal strain ($\Delta L/L$) with a slope of 0.7 (Fig. A2). Assuming infinitesimal differences $\Delta r \rightarrow dr$ and $\Delta L \rightarrow dL$ and integrating gives $\log(r/r_0) = 0.7 \log(L/L_0)$, i.e., $r/r_0 = (L/L_0)^{0.7}$. Therefore, using Eqs. 1 and 8,

$$L = \left(\frac{L_0^{7/5} M}{\pi \rho_m r_0^2 \phi}\right)^{5/12}, \tag{10}$$

and the optical density is given by

$$OD = \varepsilon \phi r_0 \left(\frac{L}{L_0}\right)^{0.7}. \tag{11}$$

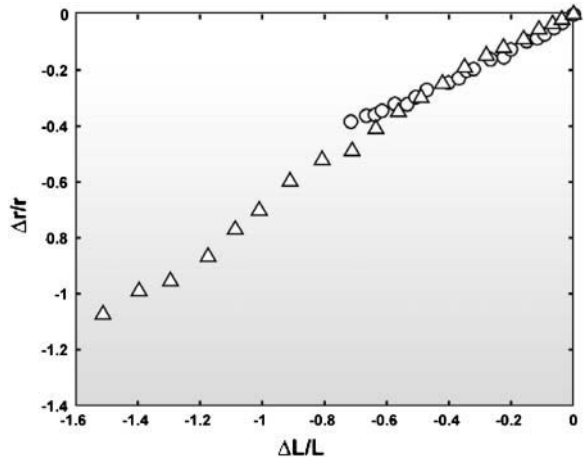

FIGURE A2 Axial strain versus longitudinal strain. The slope of the line is 0.7. Triangles are for media containing cell-free sperm extracts and YOP. Circles are for media of KPM buffer.

The effective number of monomers between cross-links

We denote by P_c the number of chains that are connected to the mesh at both ends, and by P_f the number of chains with one free end. On average, there are N_x monomers per connected chain. We denote the total number of monomers in the free chains as N_f. The total mass of the gel polymer is therefore,

$$M = \rho_m V_m (P_c N_x + N_f). \tag{12}$$

To connect the chemical kinetic Eq. 4 to the gel pressure Eq. 2, we must define N_e in terms of P_c, N_x, P_f, and N_f. Following Flory, we begin by defining the effective number of cross-links (Flory, 1953),

$$\frac{\nu_e}{2} = \frac{\nu - P_f}{2}, \tag{13}$$

where $\nu/2$ is the total number of cross-links, which can be shown to be

$$\nu = P_c + \frac{P_f}{2}. \tag{14}$$

For an isotropic, homogeneous gel, the total number of cross-links can be related to the volume fraction by

$$\nu = \frac{\phi V}{N_x V_m} - \frac{N_f}{N_x} + \frac{P_f}{2}, \tag{15}$$

where V is the volume of the gel and V_m is the volume of a monomer. If we assume that the gel is composed of flexible filaments and that the deformations are affine, the rubber elastic energy per volume of gel is (Flory, 1953)

$$\begin{aligned}\frac{F_{el}}{V} &= \left(\frac{3k_BT}{2}\right)\frac{\nu_e}{V}\left(\left(\frac{\phi_0}{\phi}\right)^{2/3} - 1 - \frac{1}{3}\ln\left(\frac{\phi_0}{\phi}\right)\right) \\ &= \left(\frac{3k_BT}{2V_m}\right)\frac{\phi(P_c - P_f)}{(N_x P_c + N_f)}\left(\left(\frac{\phi_0}{\phi}\right)^{2/3} - 1 - \frac{1}{3}\ln\left(\frac{\phi_0}{\phi}\right)\right),\end{aligned} \tag{16}$$

where we have used the relation

$$\phi V = V_m (N_x P_c + N_f). \tag{17}$$

Taking the functional derivative of this energy, we find the elastic stress,

$$\left(\frac{V_m}{k_BT}\right)\sigma_{el} = \left(\frac{P_c - P_f}{N_x P_c + N_f}\right)\left(\frac{1}{2}\phi - \phi_0^{2/3}\phi^{1/3}\right)\delta_{ij}. \tag{18}$$

Comparing Eq. 18 with Eq. 2, we find

$$\frac{1}{N_e} = \frac{P_c - P_f}{N_x P_c + N_f}, \tag{19}$$

or

$$N_e = \frac{N_x P_c + N_f}{P_c - P_f} = \frac{M}{\rho_m (P_c - P_f)}. \tag{20}$$

Note that for actin gels the expression is more complicated because the chains are semistiff, and the rubber elastic stress cannot be used.

Unbundling induced retraction forces

Whether polymer filaments are flexible or semiflexible, association into a fiber bundle will increase rigidity over the individual constituents. A fiber bundle composed of N_b polymer filaments (such as depicted in Fig. 3 *c*) will behave like a single semiflexible filament with a larger persistence length than the individual filaments. We will denote the single filament persistence length as ℓ_p and the effective persistence length of the bundle as L_p. From elasticity theory, the persistence length varies like the square of the cross-sectional area of the filament. Because the cross-sectional area of the filament bundle is proportional to the number of filaments in the bundle,

$$L_p = N_b^2 \ell_p. \tag{21}$$

Therefore, as filaments dissociate from the bundle, both N_b and the effective persistence length decrease. As suggested by the in vitro MSP experiments, we assume that the MSP filaments leave the bundle uniformly along the length of the contracting tail and assume that the number of filaments in the bundle is proportional to M_c,

$$N_b = \frac{N_0 M_c}{M_c(0)}. \tag{22}$$

This assumption does not dictate how the radius of the MSP fiber bundle changes with depolymerization. For this mechanism, it is possible that filaments either shed uniformly throughout the bulk of the fiber or preferentially at the surface. In the former case, the observed change in radius would be due to mechanical stress; whereas in the latter case, shedding of MSP filaments from the surface could be responsible for the decrease in radius. The force/extension relation for semiflexible filaments under small load force, F_L, is

$$F_L \approx \frac{90 k_B T L_p^2}{L^4}\left(L - L_\infty + \frac{L^2}{6L_p}\right), \tag{23}$$

where L is the end-to-end distance of the filament (MacKintosh et al., 1995). It should be noted that, even though this equation was derived assuming small fluctuations of a straight filament, at zero load force and with $\ell_p \ll L_\infty$, Eq. 23 gives the Flory result for the end-to-end distance of a flexible polymer chain. In addition, Eq. 23 predicts that the change in length, ΔL, is proportional to F_L for small deformations. From this relation, if F_L, L_p, and L_∞ are known, then the end-to-end distance of the filament can be calculated.

Substituting Eq. 22 into Eq. 23,

$$F_L \approx \frac{90 k_B T \ell_p^2 N_b^4}{L^4}\left(L - L_\infty + \frac{L^2}{6\ell_p N_b^2}\right). \tag{24}$$

We assume that the free filaments exert an expansive pressure on the bundled filaments proportional to the volume fraction of free filaments, ϕ_f:

$$F_L = a\phi_f = \frac{bM_f}{L^{2.4}}, \tag{25}$$

where a and b are constants. Therefore,

$$90 k_B T \ell_p^2 N_b^4 \left(L - L_\infty + \frac{L^2}{6\ell_p N_b^2}\right) \approx bM_f L^{1.6}. \tag{26}$$

Using Eqs. 5 and 22, we solved Eq. 26 for the length. Then, we used that $\phi \propto ML^{-2.4}$ to solve for the volume fraction.

Protrusion forces induced by filament bundling

Just as the unraveling of the MSP bundled filaments generate a contractile force, the bundling of filaments into thicker fibers can generate a protrusive force at the leading edge. Here we propose a mechanism by which this could happen.

Because nucleation of filaments requires a membrane associated protein (LeClaire et al., 2003), filaments nucleate and grow off the surface of the vesicle or membrane. Then, after growing to lengths of approximately a micron, the filaments detach. During this process, many of the filaments can become laterally adhered or cross-linked and form a bundled core behind the vesicle, corresponding to a protrusion (vilopod) at the cell surface (see Fig. 1 *a*). If the filaments are flexible, their Brownian thrashing can be captured by the core of the fiber (see Fig. A3). Thus, there are two sources of protrusive force. The attached filaments cannot push, but once detached they can fluctuate and exert a pressure on the surface. This mechanism is similar to the tethered elastic ratchet model (Mogilner and Oster, 2003). Also the formation of the dense core of the fiber complex acts as another kind of ''ratchet'' mechanism that rectifies fluctuations of the membrane (or cell surface). Thus, as the fiber elongates, it forms a barrier to backwards motion. This ratchet-induced forward motion is driven by lateral association of the filaments rather than polymerization as in the actin system.

Consider the system shown in Fig. A3 where N filaments zip up via lateral binding interactions against a load force, F_L. A quantitative model can be created by treating the bundled portion of the filaments as a single semiflexible polymer. The unbundled end can be treated in one of two ways, depending on the stiffness of the filaments. If the single polymer filaments are flexible, then they can be treated as a polymer brush: an arrangement of polymer chains where one end of each chain is grafted to a surface and the other end is free. If the individual polymers are semistiff, like actin, then the MacKintosh relation (Eq. 23) can be used. The length of the filament bundle, L_b, is also determined from Eq. 23. For the polymer brush, assuming that the individual polymer chains in the brush are not entangled, the length of the polymer brush, L_{pb}, can be calculated from mean-field theory (Marsh, 2004)

$$F_L = \alpha\lambda^{-2}A_{pb}\left(\frac{D}{a_m}\right)^{1/3}\left(\frac{k_BT}{D}\right)\left(\left(\frac{L_0}{L_{pb}}\right)^2 - \frac{L_{pb}}{L_0}\right), \qquad (27)$$

where α and λ are constants and A_{pb} is the cross-sectional area. The monomer radius is a_m and D is the spacing between polymers. The equilibrium length of the polymer brush is

$$L_0 = \lambda a_m m\left(\frac{a_m}{D}\right)^{2/3}, \qquad (28)$$

where m is the number of monomers per polymer chain in the brush. The contour length of the polymers in the brush is $L_c = a_m m = L_0 D^{2/3}/\lambda a_m^{2/3}$, and the total length of the polymers in the combined bundle and brush is $L_{con} = L_c + L_\infty$ and the length of the composite object is $L_T = L_b + L_{pb}$.

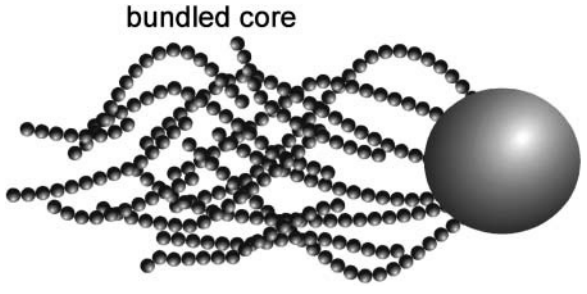

FIGURE A3 Protrusion forces. At the leading edge MSP polymerization elongates the filaments, while lateral association elongates the fiber bundles whose persistence length is much higher than the filaments. The fluctuating filaments impinge on the leading edge membrane, and so their entropic freedom is reduced. This generates a protrusive pressure on the leading edge and a compressive stress in the filament bundles whose bending modulus is large enough to transmit the stress rearwards and to the substratum.

Lateral binding increases L_∞ and decreases L_c thereby increasing the object length, L_T. Defining the growth rates of L_∞ and L_c completes the model.

The authors thank Mark Zajac for useful discussions.

C.W. was supported by National Science Foundation grant MCB-0327716. G.O. was supported by National Science Foundation grant DMS-9972826. T.R. was supported by National Institutes of Health grant R37 GM29994.

REFERENCES

Abercrombie, M. 1980. The Croonian lecture, 1978. The crawling movement of metazoan cells. *Proc. R. Soc. Lond. B Biol. Sci.* 207:129–147.

Bottino, D., A. Mogilner, M. Stewart, and G. Oster. 2001. How nematode sperm crawl. *J. Cell Sci.* 115:367–384.

Brieher, W. M., M. Coughlin, and T. J. Mitchison. 2004. Fascin-mediated propulsion of Listeria monocytogenes independent of frequent nucleation by the Arp2/3 complex. *J. Cell Biol.* 165:233–242.

Bullock, T. L., T. M. Roberts, and M. Stewert. 1996. 2.5 Angstrom resolution crystal structure of the motile major sperm protein (MSP). *J. Mol. Biol.* 263:284–296.

Cameron, L. A., M. J. Footer, A. V. Oudenaarden, and J. A. Theriot. 1999. Motility of ActA protein-coated microspheres driven by actin polymerization. *Proc. Natl. Acad. Sci. USA.* 96:4908–4913.

Cameron, L. A., P. A. Giardinia, F. S. Soo, and J. A. Theriot. 2000. Secrets of actin-based motility revealed by a bacterial pathogen. *Nat. Rev. Mol. Cell Biol.* 1:110–119.

DeLozanne, A., and J. A. Spudich. 1987. Disruption of the Dictyostelium myosin heavy chain gene by homologous recombination. *Science.* 236:1086–1091.

English, A. E., S. Mafe, J. A. Manzanares, Y. Xiahong, A. Y. Grosberg, and T. Tanaka. 1996a. Equilibrium swelling properties of polyampholytic hydrogels. *J. Chem. Phys.* 104:8713–8720.

English, A. E., T. Tanaka, and E. R. Edelman. 1996b. Polyelectrolyte hydrogel instabilities in ionic solutions. *J. Chem. Phys.* 105:10606–10613.

Flory, P. 1953. Principles of Polymer Chemistry. Cornell University Press, Ithaca, NY.

Gardel, M. L., J. H. Shin, F. C. MacKintosh, L. Mahadevan, P. Matsudaira, and D. A. Weitz. 2004. Elastic behavior of cross-linked and bundled actin networks. *Science.* 304:1301–1305.

Gaudet, C., W. A. Marganski, S. Kim, C. T. Brown, V. Gunderia, M. Dembo, and J. Y. Wong. 2003. Influence of type I collagen density on fibroblast spreading, motility, and contractility. *Biophys. J.* 85:3329–3335.

Herant, M., W. A. Marganski, and M. Dembo. 2003. The mechanics of neutrophils: synthetic modeling of three experiments. *Biophys. J.* 84: 3389–3413.

Huxley, H. E. 1973. Muscular contraction and cell motility. *Nature.* 243:445–449.

Italiano, J. E., T. M. Roberts, M. Stewart, and C. A. Fontana. 1996. Reconstruction in vitro of the motile apparatus from the amoeboid sperm *Ascaris* shows that filament assembly and bundling move membranes. *Cell.* 84:105–114.

Joanny, J. F., F. Julicher, and J. Prost. 2003. Motion of an adhesive gel in a swelling gradient: a mechanism for cell locomotion. *Phys. Rev. Lett.* 90:168102.

Knecht, D. A., and W. F. Loomis. 1987. Antisense RNA inactivation of myosin heavy chain gene expression in Dictyostelium discoideum. *Science.* 236:1081–1086.

Koo, L. Y., D. J. Irvine, A. M. Mayes, D. A. Lauffenburger, and L. G. Griffith. 2002. Co-regulation of cell adhesion by nanoscale RGD organization and mechanical stimulus. *J. Cell Sci.* 115:1423–1433.

Lauffenburger, D. A., and A. F. Horwitz. 1996. Cell migration: a physically integrated molecular process. *Cell*. 84:359–369.

LeClaire, L. L., M. Stewart, and T. M. Roberts. 2003. A 48 kDa integral membrane phosphoprotein orchestrates the cytoskeletal dynamics that generate amoeboid cell motility in Ascaris sperm. *J. Cell Sci*. 116:2655–2663.

MacKintosh, F. C., J. Kas, and P. A. Janmey. 1995. Elasticity of semiflexible biopolymer networks. *Phys. Rev. Lett*. 75:4425–4428.

Marcy, Y., J. Prost, M.-F. Carlier, and C. Sykes. 2004. Forces generated during actin-based propulsion: a direct measurement by micromanipulation. *Proc. Natl. Acad. Sci. USA*. 101:5992–5997.

Marsh, D. 2004. Scaling and mean-field theories applied to polymer brushes. *Biophys. J*. 86:2630–2633.

Miao, L., O. Vanderlinde, M. Stewart, and T. M. Roberts. 2003. Retraction in amoeboid cell motility powered by cytoskeletal dynamics. *Science*. 302:1405–1407.

Mitchison, T. J., and L. P. Cramer. 1996. Actin-based cell motility and cell locomotion. *Cell*. 84:371–379.

Mogilner, A., and G. Oster. 1996. The physics of lamellipodial protrusion. *Euro. Biophys. J*. 25:47–53.

Mogilner, A., and G. Oster. 2003. Force generation by actin polymerization II: the elastic ratchet and tethered filaments. *Biophys. J*. 84:1591–1605.

Mogilner, A., and D. W. Verzei. 2003. A simple 1-D model for the crawling nematode sperm cell. *J. Stat. Phys*. 110:1169–1189.

Oliver, T., J. Lee, and K. Jacobson. 1994. Forces exerted by locomoting cells. *Semin. Cell Biol*. 5:139–147.

Oster, G., and A. Perelson. 1988. The physics of cell motility. *In* Cell Behavior: Shape, Adhesion and Motility. J. Heaysman C. Middleton, and F. Watt, editors. The Company of Biologists, Cambridge, UK. 35–54.

Oster, G., and A. Perelson. 1994. Cell protrusions. *In* Frontiers in Mathematical Biology. S. Levin, editor. Springer-Verlag, Berlin. 53–78.

Peskin, C., G. Odell, and G. Oster. 1993. Cellular motions and thermal fluctuations: the Brownian ratchet. *Biophys. J*. 65:316–324.

Rahman, A., Y. Tseng, and D. Wirtz. 2002. Micromechanical coupling between cell surface receptors and RGD peptides. *Biochem. Biophys. Res. Commun*. 296:771–778.

Roberts, T. M., and M. Stewert. 1997. Nematode sperm amoeboid movement without actin. *Trends Cell Biol*. 7:368–373.

Sepsenwol, S., H. Ris, and T. M. Roberts. 1989. A unique cytoskeleton associated with crawling in the amoeboid sperm of the nematode, Ascaris suum. *J. Cell Biol*. 108:55–66.

Svitkina, T. M., E. A. Bulanova, O. Y. Chaga, D. M. Vignjevic, S. Kojima, J. M. Vasiliev, and G. G. Borisy. 2003. Mechanism of filopodia initiation by reorganization of a dendritic network. *J. Cell Biol*. 160:409–421.

Theriot, J. A., J. Rosenblatt, D. A. Portnoy, P. J. Goldshmidt-Clermont, and T. J. Mitchison. 1994. Involvement of profilin in the actin-based motility of L. monocytogenes in cells and in cell-free extracts. *Cell*. 76:505–517.

Watanabe, N., and T. J. Mitchison. 2002. Single-molecule speckle analysis of actin filament turnover in lamellipodia. *Science*. 295:1083–1085.

Wolgemuth, C. W., A. Mogilner, and G. Oster. 2004. The hydration dynamics of polyelectrolyte gels with applications to drug delivery and cell motility. *Eur. Biophys. J*. 33:146–158.